Static magnetic order on the metallic triangular lattice in $CrSe_2$ detected by μ^+SR

Jun Sugiyama,[1,2,*] Hiroshi Nozaki,[1] Izumi Umegaki,[1] Takeshi Uyama,[1] Kazutoshi Miwa,[1] Jess H. Brewer,[3,4] Shintaro Kobayashi,[5] Chishiro Michioka,[5] Hiroaki Ueda,[5] and Kazuyoshi Yoshimura[5]

[1]*Toyota Central Research & Development Laboratories, Inc., Nagakute, Aichi, 480-1192 Japan*

[2]*Advanced Science Research Center, Japan Atomic Energy Agency, Tokai, Ibaraki, 319-1195 Japan*

[3]*TRIUMF, 4004 Wesbrook Mall, Vancouver, BC, V6T 2A3 Canada*

[4]*Department of Physics & Astronomy, University of British Columbia, Vancouver, BC, V6T 1Z1 Canada*

[5]*Department of Chemistry, Graduate School of Science, Kyoto Univ., Kyoto, 606-8502 Japan*

(Received 8 May 2016; revised manuscript received 14 June 2016; published 7 July 2016)

The magnetic nature of a metallic two-dimensional triangular compound, $CrSe_2$, has been investigated by muon spin rotation and relaxation (μ^+SR) measurements using both powder and single crystal samples. It is found that $CrSe_2$ enters into a static antiferromagnetic (AF) ordered state below 157 K ($=T_N$). Furthermore, the AF state is slightly changed below around 20 K ($=T_{N2}$). Based on the analysis of the internal magnetic fields at the muon sites predicted with DFT calculations, collinear AF and helical 120° AF are clearly eliminated for the ground state of $CrSe_2$. The most probable one is an incommensurate spin density wave order.

DOI: 10.1103/PhysRevB.94.014408

I. INTRODUCTION

For compounds having a two-dimensional triangular lattice (2DTL), on which each corner is occupied by a magnetic moment, when the interaction between the two neighboring moments is antiferromagnetic (AF), it is impossible to satisfy all AF interactions. As a result, such geometrical frustration often leads to exotic magnetic transitions.

A chromium selenide, $1T$-$CrSe_2$, belongs to a layered transition-metal dichalcogenides $1T$-MX_2 family with 2DTL [1,2], where M is a transition metal and X is a chalcogen (S, Se, Te). $1T$ means the phase with the layered CdI_2 structure, in which M ions form the 2DTL by the connection of edge-sharing MX_6 octahedra (Fig. 1).

Among them, $1T$-$TiSe_2$ is known to exhibit a transition to a charge density wave (CDW) state with a $2a \times 2a \times 2c$ superlattice at $T_{CDW} = 202$ K [4–7]. As a result, resistivity (ρ) starts to increase with decreasing T at T_{CDW} and reaches a maximum around 150 K, while susceptibility (χ) shows a sudden decrease at T_{CDW} and becomes almost T independent below around 100 K [4]. Recent discovery of superconductivity with $T_c = 1.8$ K under high pressures between 2 and 4 GPa attracted great attention on the interplay between superconductivity and the CDW state [8].

The isostructural compound $1T$-VSe_2 also exhibits a CDW transition at $T_{CDW} = 112$ K [9,10]. The lattice modulation is commensurate (C) in the c plane ($4a \times 4a$), but incommensurate (IC) along the c axis ($3.3c$) [11–13]. As T is further decreased, a lock-in transition to a C phase with a superlattice $3a \times 3a \times 3c$ is likely to occur at $T_{lock} \sim 60$ K [14]. The $\rho(T)$ and $\chi(T)$ curves exhibit roughly a similar behavior at T_{CDW} [9] as those for $1T$-$TiSe_2$.

$1T$-$CrSe_2$ was found to undergo successive phase transitions at 180 and 160 K [1]. That is, as T decreases from room T, χ increases abruptly at $T_{t1} = 186$ K and $T_{t2} = 164$ K, but the changes in ρ at these temperatures are less drastic than χ and $1T$-$CrSe_2$ is metallic down to 2 K [1,2]. These behaviors are different from those observed at T_{CDW} for $1T$-$TiSe_2$ and $1T$-VSe_2, suggesting other mechanisms for the transitions are operative in $1T$-$CrSe_2$. Furthermore, very recent magnetization measurements on $1T$-$Cr_{1-x}V_xSe_2$ and $1T$-$Cr_{1-x}Ti_xSe_2$ indicated that the phase below 186 K is not a CDW state but an AF ordered state [15], although there is no neutron diffraction data to corroborate this possibility. This would mean the formation of a spin density wave order (SDW) for $1T$-$CrSe_2$ instead. Based on electron diffraction measurements and XRD analyses [2], a high-T trigonal phase with space group $P\bar{3}m1$ was found to transform into a low-T rhombohedral phase with $R\bar{3}m$ through a monoclinic phase with $I2/m$, probably due to the spin-orbit coupling for a t_{2g}^2 electron system.

Note that it is difficult to measure ^{77}Se-NMR due to the low natural abundance of this isotope (7.63%). For the same reason—i.e. the natural abundance of ^{53}Cr is 9.50%, ^{53}Cr-NMR is not a suitable technique particularly for AF materials. Furthermore, since the typical size of the crystals obtained is $0.3 \times 0.3 \times 0.1$ mm^3 [2], it is currently impossible to prepare enough amount of samples for neutron diffraction measurements. As a result, the ground state of $1T$-$CrSe_2$ is

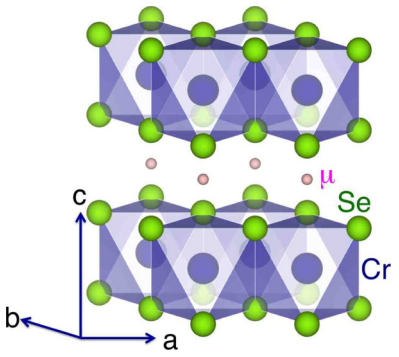

FIG. 1. The crystal structure of $1T$-$CrSe_2$ drawn with VESTA [3]. The muon site was predicted at (0, 0, 1/2), which is the middle of the two neighboring Cr ions along the c axis, by DFT calculations (see text).

*e0589@mosk.tytlabs.co.jp

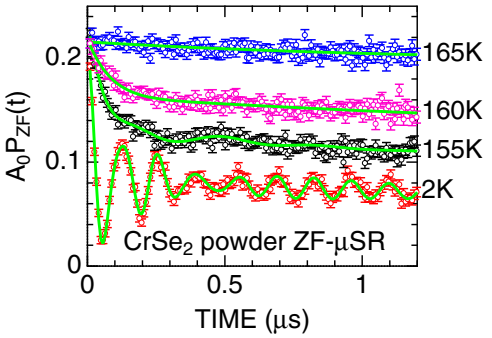

FIG. 2. The temperature variation of the ZF-μ^+SR spectrum in $1T$-$CrSe_2$. Solid lines represent the fit result using Eq. (1).

still unknown [1,2,15,16], despite a relatively simple crystal structure. We have therefore measured muon spin rotation and relaxation (μ^+SR) spectra of $1T$-$CrSe_2$ to understand its magnetic ground state.

II. EXPERIMENTAL

The preparation of the $1T$-$CrSe_2$ sample was already reported elsewhere [2]. The μ^+SR time spectra were measured at the surface muon beam line M20 using the LAMPF spectrometer of TRIUMF in Canada. The approximately 100 mg powder sample was placed in an envelope with 1 cm^2 area, made of 0.05 mm thick Al-coated Mylar tape in order to minimize the signal from the envelope. Also, about 50 pieces of single crystal platelets were stacked between Mylar tapes so as to align the c axis perpendicular to the tape plane. The envelope or tape was then attached to a low-background sample holder in a liquid-He flow-type cryostat for measurements in the T range between 1.8 and 220 K. The experimental techniques are described in more detail elsewhere [17,18].

III. RESULTS

In order to know whether static magnetic order exists in $1T$-$CrSe_2$ at low T, Fig. 2 shows the T variation of the μ^+SR spectrum recorded in a zero external field (ZF). Since the ZF-μ^+SR spectrum at 165 K looks almost time independent until 1 μs, $CrSe_2$ is in a paramagnetic state. At 160 K, however, a rapidly relaxing component appears in an early time domain, and such component changes into an oscillatory signal at 155 K. At 1.8 K, which is the lowest T measured, a muon spin precession signal is clearly observed, which unambiguously indicates the formation of quasistatic AF order in $1T$-$CrSe_2$.

Figure 3 shows the Fourier transform of the ZF-μ^+SR time spectrum to understand the change in the internal magnetic fields with T. There are three distinct frequencies at temperatures below around 140 K, although it is hard to distinguish the three frequencies above 140 K. Therefore, the ZF-μ^+SR time spectrum was fitted by a combination of three exponentially relaxing cosine oscillations for the quasistatic AF internal fields, an exponentially relaxing nonoscillatory signal for the "1/3 tail" signal caused by fluctuations in the field component parallel to the initial muon spin polarization, and an additional exponentially relaxing nonoscillatory signal from the muons stopped in a paramagnetic second phase and/or

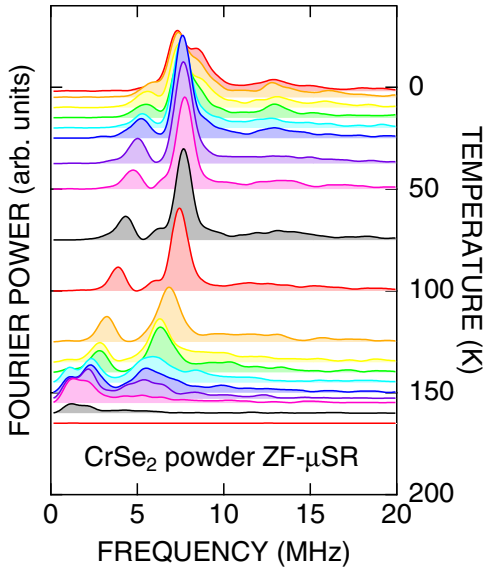

FIG. 3. The temperature dependence of the Fourier transform frequency spectrum of the ZF-μ^+SR time spectrum for $1T$-$CrSe_2$.

a surrounding sample holder and cryostat:

$$A_0\,P_{ZF}(t) = \sum_{i=1}^{3}[A_{AFi}e^{-\lambda_{AFi}t}\cos(\omega_{AFi}t+\phi_{AFi})] + A_{tail}e^{-\lambda_{tail}t} + A_{2nd}e^{-\lambda_{2nd}t}\,. \quad (1)$$

Here A_0 is the initial asymmetry, $P_{ZF}(t)$ is the muon spin depolarization function in ZF, A_{AFi}, A_{tail}, and A_{2nd} are the asymmetries associated with the five signals, $f_{AFi}(\equiv\omega_{AFi}/2\pi)$ are the muon Larmor frequencies corresponding to the quasistatic internal AF fields, λ_{AFi}, λ_{tail}, and λ_{2nd} are their exponential relaxation rates, and ϕ_{AFi} are the initial phases.

Figure 4 shows the T dependences of the μ^+SR parameters together with $\chi(=M/H)$ measured at $H=5$ kOe. As T increases from 1.8 K, both f_{AF1} and f_{AF2} are almost T independent up to ~75 K, and decreases with increasing slope (df_{AF}/dT), then f_{AF1} merges into f_{AF2} at ~140 K, and finally disappears at ~160 K ($=T_N$). On the contrary, f_{AF3} rapidly decreases with T until ~20 K, and then decreases slowly with T, and finally drops to 0 at T_N. This indicates the presence two AF transitions at 160 and 20 K ($=T_{N2}$).

Three A_{AFi}s show a complex T dependence below ~20 K, but are roughly T independent above 20 K besides below the vicinity of T_N, and abruptly disappear at T_N. However, $\sum A_{AFi}$ is ~2/3 (A_{tail} is ~1/3) of $[\sum A_{AFi}+A_{tail}]$ below T_N, as expected. The T dependences of A_{AFi}s below T_{N2} would suggest a slight structural variation in these T. The magnitude of A_{2nd} was about 15% of a total asymmetry ($0.22=A_0$) and roughly independent of T below T_N, as described later.

Besides the vicinity of T_N, both ϕ_{AF2} and ϕ_{AF3} increase with decreasing T and reach a maximum at around T_{N2}, while ϕ_{AF1} shows an opposite T dependence. Below T_{N2}, although ϕ_{AF2} approaches to zero with further decreasing T, $\phi_{AF1}=-18(9)^\circ$ and $\phi_{AF2}=-26(6)^\circ$ even at 2 K. Such delay is sometimes an evidence for IC-SDW order [17,19–21], and we will discuss a possible AF structure later.

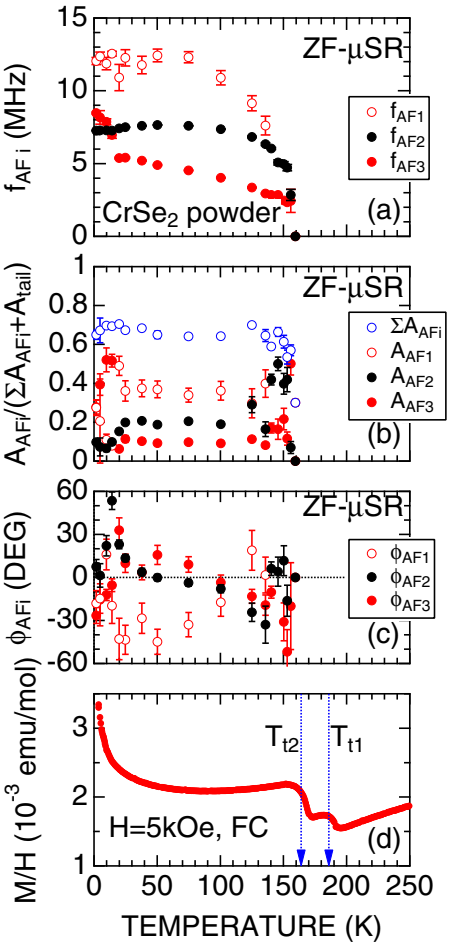

FIG. 4. T dependences of (a) the muon spin precession frequencies for the A_{AFi} signal (f_{AFi}); (b) the normalized asymmetries (A_{AFi} and A_{tail} divided by $\sum A_{AFi} + A_{tail}$); (c) the initial phases for the A_{AFi} signal (ϕ_{AFi}); (d) $\chi = M/H$ for $1T$-$CrSe_2$. The χ data were obtained in field cooling (FC) mode with $H = 5$ kOe.

Making comparison with the $\chi(T)$ curve, the present μ^+SR results clearly demonstrate that the bulk AF transition does not occur at T_{t1} but at $T_{t2}(= T_N)$. Furthermore, the increase in χ at low T, particularly below ~20 K, is consistent with T_{N2} found with μ^+SR.

Figure 5 shows the T dependences of the μ^+SR parameters obtained from weak transverse field (wTF-) measurements with $H_{TF} = 30$ Oe together with the ZF-μ^+SR measurements. Here, wTF means the field is perpendicular to the initial muon spin polarization and its magnitude is very small compared with the internal magnetic field (H_{int}) generated by magnetic order and/or disorder. The wTF-spectra were fitted by:

$$A_0\, P_{TF}(t) = A_{TF}\cos(\omega_{TF}t + \phi)e^{-\lambda_{TF}t} + A_M e^{-\lambda_M t}, \quad (2)$$

where A_{TF} and A_M are the asymmetries for the oscillatory signal due to applied wTF and the nonoscillatory relaxing signal caused by localized magnetic moments. In addition, the ZF-μ^+SR spectrum measured at $T > T_N$ was fitted by a single exponential relaxing signal, namely, $A_0 P_{ZF}(t) = A_{ZF}e^{-\lambda_{ZF}t}$.

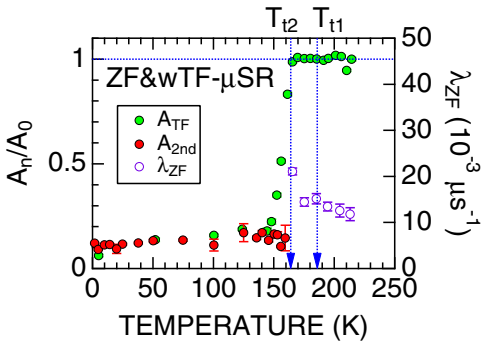

FIG. 5. T dependences of the two normalized asymmetries, A_{TF}/A_0 and A_{2nd}/A_0, and the exponential relaxation rate λ_{ZF}. A_{TF} was obtained by fitting wTF-μ^+SR spectra using Eq. (2). A_{2nd} was estimated by fitting ZF-μ^+SR spectra below T_N using Eq. (1), whereas λ_{ZF} by fitting ZF-μ^+SR spectra above T_N with $A_{ZF}e^{-\lambda_{ZF}t}$.

As seen in Fig. 5, the $A_{TF}/A_0(T)$ curve, where A_{TF}/A_0 corresponds to the volume fraction of paramagnetic phases in a sample, shows a steplike change at ~160 K from 1 to about 0.15 with decreasing T. This means that 85% volume of the sample becomes AF below T_N, but the rest 15% is paramagnetic even at 1.8 K. Furthermore, A_{TF}/A_0 is roughly T independent below T_N and is equal to A_{2nd}/A_0 extracted from the ZF data. From the $A_{TF}/A_0(T)$ curve, $T_N^{\mu SR}$ is estimated as 157.4 K, at which $A_{TF}/A_0 = 1 - (0.85/2)$. Concerning the situation at T_{t1}, there is no crucial change in both A_{TF} and λ_{ZF}, indicating that T_{t1} is not a magnetic but electronic and/or structural transition.

In order to know the magnetic anisotropy of the AF phase, Fig. 6 shows the ZF-μ^+SR spectra for the single crystal platelets of $1T$-$CrSe_2$ with two different configurations, namely, $\boldsymbol{S}_\mu(0) \parallel \boldsymbol{c}$ and $\boldsymbol{S}_\mu(0) \perp \boldsymbol{c}$, where $\boldsymbol{S}_\mu(0)$ is the direction of the initial muon spin. The strongest signal at 2 K, i.e., the A_{AF3} signal is clearly observed with both configurations. This means that H_{int} of the A_{AF3} signal is neither parallel nor perpendicular to the ab plane. The cant angle from the ab plane [$\Theta_{AF3} \equiv \tan^{-1}(A_{AF3}^{\boldsymbol{S}_\mu(0)\perp\boldsymbol{c}}/A_{AF3}^{\boldsymbol{S}_\mu(0)\parallel\boldsymbol{c}})$] was about 38°.

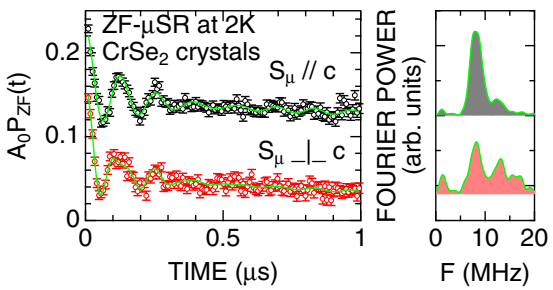

FIG. 6. ZF-μ^+SR time spectra at 2 K for $1T$-$CrSe_2$ crystals: top: $\boldsymbol{S}_\mu(0) \parallel \boldsymbol{c}$; bottom: $\boldsymbol{S}_\mu(0) \perp \boldsymbol{c}$. Top spectrum is offset by 0.1 for display clarity. Solid lines represent fits using Eq. (1) with common λ_i and ω_{AFi}. The right panel shows Fourier transforms of the ZF time spectra.

IV. DISCUSSION

The electrostatic potential distribution predicted by DFT calculations with generalized gradient approximation (GGA) [22] suggests that the implanted muons sit at the 1*b* site, (0, 0, 1/2), which is the middle of the two neighboring Cr ions in the adjacent $CrSe_2$ planes (see Fig. 1 and Appendix).

Although the present calculations *do not* consider the lattice relaxation due to the implanted μ^+, the predicted muon site is the same as that of Na^+ in $NaCrSe_2$ [23]. Since $NaCrSe_2$ is assigned as a Na intercalated $CrSe_2$, the predicted muon site is thought to be reasonable in $CrSe_2$.

Then, dipole field calculations (Table I) show that $H_{\rm int} = 0$ for both A-type and G-type AF order. Here, Cr moments ($\boldsymbol{M}_{\rm Cr}$s) align parallel in the *ab* plane but antiparallel along the *c* axis for A-type AF, while $\boldsymbol{M}_{\rm Cr}$s align antiparallel in the *ab* plane and along the *c* axis for G-type AF. Even for C-type AF order, in which $\boldsymbol{M}_{\rm Cr}$s align antiparallel in the *ab* plane but parallel along the *c* axis, there is only one unique $H_{\rm int}$. Moreover, the experimental results are not explained by a helical 120° AF structure along the *c* axis.

The present μ^+SR result, therefore, indicates a more complex AF spin structure in 1*T*-$CrSe_2$ rather than simple collinear [15] and 120° AF spin structures. Considering the metallic AF nature of 1*T*-$CrSe_2$ and the delay of $\phi_{{\rm AF}i}$, a helical IC-SDW order, which is predicted for 2DTL [25] and found in several materials [26–28], is thought to be the most reasonable AF structure.

In fact, due to the mismatch between the AF modulation period and lattice period, IC-SDW order is known to generate multiple frequencies in the ZF-μ^+SR spectrum, even in the case that there is crystallographically one muon site. However, in order to explain nonzero Θ, the AF spin would be canted from the *ab* plane.

TABLE I. Dipole field ($H_{\rm int}$) and its cant angle from the *ab* plane (Θ) at the muon site with three collinear and 120° AF structures estimated with DipElec [24]. For G and C-type AF, Cr moments ($\boldsymbol{M}_{\rm Cr}$s) align antiparallel along the *a* axis, but parallel along the *b* axis. "60° helical along (001)" means that each $\boldsymbol{M}_{\rm Cr}$ of the 120° AF structure in the $CrSe_2$ plane rotates by 60° in the adjacent $CrSe_2$ plane along the *c* axis.

AF		$H_{\rm int}/M_{\rm Cr}$ (Oe/$\mu_{\rm B}$)	Θ (DEG)
A	$M_{\rm Cr} \parallel$ (100)	0	
	$M_{\rm Cr} \parallel$ (001)	0	
G	$M_{\rm Cr} \parallel$ (100)	0	
	$M_{\rm Cr} \parallel$ (001)	0	
C	$M_{\rm Cr} \parallel$ (100)	947	0
	$M_{\rm Cr} \parallel$ (001)	1286	90
	$M_{\rm Cr} \parallel$ (101)	1129	54
120°	parallel along (001)	602	0
	60° helical along (001)	521	0
	120° helical along (001)	300	0
	180° helical along (001)	0	
		$H_{\rm int}$ (Oe)	Θ (DEG)
experiment	2 K	540, 597, 908	24, 38, 84
	28 K	393, 559, 940	38, 36, 90

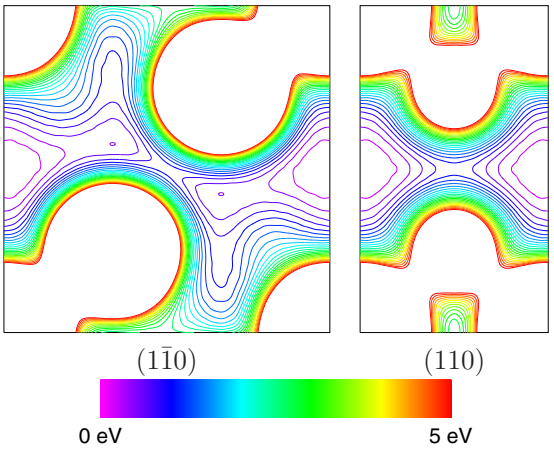

FIG. 7. Contour plots of the electrostatic potential in FM-$CrSe_2$. The potential at the muon site is set to be zero. Contour spacing is 0.2 eV and lines are omitted for the potentials higher then 5 eV.

Here, we ignored a slight spatial displacement of Cr ions at low *T* found by electron diffraction observations [2], because such structural data are unavailable at present. However, the displacement of Cr ions, particularly along the *c* axis may affect both $H_{\rm int}$ and Θ.

When 1/3 of Cr ions are displaced along the *c* axis by 1%, 1/3 by −1%, and the remaining 1/3 are not displaced, there is still one $H_{\rm int}$ for the 120° AF spin structure with parallel along (001), but three $H_{\rm int}$s for the 120° AF spin structure 180° helical along (001). However, Θ is still ∼0 for both cases. This supports the above conclusion that the simple AF structures are excluded, even when the implanted muons slightly alter local structural circumstances. In order to further clarify the ground state of 1*T*-$CrSe_2$, we need to perform both synchrotron x-ray and neutron diffraction analyses using a high quality sample in the wide *T* range.

ACKNOWLEDGMENTS

We thank the staff of TRIUMF (especially the CMMS) for help with the μ^+SR experiments. This work was supported by the Ministry of Education, Culture, Sports, Science and Technology (MEXT) of Japan, KAKENHI Grant No. 23108003 and Japan Society for the Promotion Science (JSPS) KAKENHI Grant No. 26286084.

APPENDIX: DFT CALCULATIONS

The electrostatic potential analysis has been performed to determine the muon site in $CrSe_2$. A self consistent field (SCF) calculation is carried out within the ultrasoft pseudopotential method [29,30] based on density functional theory [31,32], and the obtained pseudo SCF charge density is transformed into an all electron form with the projector augmented wave operators [33]. The cutoff energies of plane waves are set to be 15 and 120 hartrees for the pseudo wave functions and the charge density, respectively. The $8 \times 8 \times 4$ *k*-point mesh is adopted for the primitive hexagonal unit cell and equivalent ones for the supercells which are used to simulate AF orders. The generalized gradient approximation [34,35] is used for the exchange-correlation functional. In the structural optimization

process, lattice constants are fixed at the experimental values ($a = 3.40$ Å and $c = 5.91$ Å) [2] and atomic positions are only optimized.

According to Ref. [15], we consider the three AF structures as well as a ferromagnetic (FM) one. In all cases, the electrostatic potential analyses suggest that the muon site is the middle of the neighboring Cr atoms along the c axis. Figure 7 shows the electrostatic potential in FM-$CrSe_2$. The potential distribution in the AF structures is essentially the same as that in the FM structure.

[1] C. van Bruggen, R. Haange, G. Wiegers, and D. de Boer, Physica B+C **99**, 166 (1980).

[2] S. Kobayashi, H. Ueda, D. Nishio-Hamane, C. Michioka, and K. Yoshimura, Phys. Rev. B **89**, 054413 (2014).

[3] K. Momma and F. Izumi, J. Appl. Crystallogr. **41**, 653 (2008).

[4] F. J. Di Salvo, D. E. Moncton, and J. V. Waszczak, Phys. Rev. B **14**, 4321 (1976).

[5] R. Dupree, W. W. Warren, and F. J. DiSalvo, Phys. Rev. B **16**, 1001 (1977).

[6] A. Zunger and A. J. Freeman, Phys. Rev. Lett. **40**, 1155 (1978).

[7] N. G. Stoffel, S. D. Kevan, and N. V. Smith, Phys. Rev. B **31**, 8049 (1985).

[8] A. F. Kusmartseva, B. Sipos, H. Berger, L. Forró, and E. Tutiš, Phys. Rev. Lett. **103**, 236401 (2009).

[9] C. van Bruggen and C. Haas, Solid State Commun. **20**, 251 (1976).

[10] V. N. Strocov, M. Shi, M. Kobayashi, C. Monney, X. Wang, J. Krempasky, T. Schmitt, L. Patthey, H. Berger, and P. Blaha, Phys. Rev. Lett. **109**, 086401 (2012).

[11] K. Tsutsumi, T. Sambongi, A. Toriumi, and S. Tanaka, Physica B+C **105**, 419 (1981).

[12] K. Tsutsumi, Phys. Rev. B **26**, 5756 (1982).

[13] B. Giambattista, C. G. Slough, W. W. McNairy, and R. V. Coleman, Phys. Rev. B **41**, 10082 (1990).

[14] T. Tsuda, Y. Kitaoka, and H. Yasuoka, Physica B+C **105**, 414 (1981).

[15] D. C. Freitas, M. Núñez, P. Strobel, A. Sulpice, R. Weht, A. A. Aligia, and M. Núñez-Regueiro, Phys. Rev. B **87**, 014420 (2013).

[16] C. M. Fang, C. F. van Bruggen, R. A. de Groot, G. A. Wiegers, and C. Haas, J. Phys.: Condens. Matter **9**, 10173 (1997).

[17] G. M. Kalvius, D. R. Noakes, and O. Hartmann, *Handbook on the Physics and Chemistry of Rare Earths* (North-Holland, Amsterdam, 2001), Vol. 32, Chap. 206, pp. 55–451.

[18] A. Yaouanc and P. D. de Réotier, *Muon Spin Rotation, Relaxation, and Resonance, Application to Condensed Matter* (Oxford, New York, 2011).

[19] D. Andreica, Ph.D. thesis, ETH Zurich, 2001.

[20] J. Sugiyama, H. Nozaki, Y. Ikedo, P. L. Russo, K. Mukai, D. Andreica, A. Amato, T. Takami, and H. Ikuta, Phys. Rev. B **77**, 092409 (2008).

[21] J. Sugiyama, M. Månsson, Y. Ikedo, T. Goko, K. Mukai, D. Andreica, A. Amato, K. Ariyoshi, and T. Ohzuku, Phys. Rev. B **79**, 184411 (2009).

[22] T. Sato, K. Miwa, Y. Nakamori, K. Ohoyama, H.-W. Li, T. Noritake, M. Aoki, S.-i. Towata, and S.-i. Orimo, Phys. Rev. B **77**, 104114 (2008).

[23] W. Rüdorff, W. R. Ruston, and A. Scherhaufer, Acta Crystallogr. **1**, 196 (1948).

[24] K. M. Kojima, J. Yamanobe, H. Eisaki, S. Uchida, Y. Fudamoto, I. M. Gat, M. I. Larkin, A. Savici, Y. J. Uemura, P. P. Kyriakou *et al.*, Phys. Rev. B **70**, 094402 (2004).

[25] H. R. Krishnamurthy, C. Jayaprakash, S. Sarker, and W. Wenzel, Phys. Rev. Lett. **64**, 950 (1990).

[26] G. Grüner, *Density Waves in Solids* (Addison-Wesley-Longmans, Reading, 1994).

[27] J. Sugiyama, Y. Ikedo, T. Goko, E. J. Ansaldo, J. H. Brewer, P. L. Russo, K. H. Chow, and H. Sakurai, Phys. Rev. B **78**, 224406 (2008).

[28] H. Nozaki, J. Sugiyama, M. Månsson, M. Harada, V. Pomjakushin, V. Sikolenko, A. Cervellino, B. Roessli, and H. Sakurai, Phys. Rev. B **81**, 100410 (2010).

[29] D. Vanderbilt, Phys. Rev. B **41**, 7892 (1990).

[30] K. Miwa, Phys. Rev. B **84**, 094304 (2011).

[31] P. Hohenberg and W. Kohn, Phys. Rev. **136**, B864 (1964).

[32] W. Kohn and L. J. Sham, Phys. Rev. **140**, A1133 (1965).

[33] P. E. Blöchl, Phys. Rev. B **50**, 17953 (1994).

[34] J. P. Perdew, K. Burke, and M. Ernzerhof, Phys. Rev. Lett. **77**, 3865 (1996).

[35] J. P. Perdew, K. Burke, and M. Ernzerhof, Phys. Rev. Lett. **78**, 1396 (1997).